ACS APPLIED NANO MATERIALS

www.acsanm.org

Article

Naturally Occurring Halloysite Nanotubes as Light Scatterers for Stable Random Lasing Applications

Ashim Pramanik, Alice Sciortino, Marco Reale, Pooria Pasbakhsh, Giuseppe Cavallaro, Marco Cannas, Giuseppe Lazzara, and Fabrizio Messina*

Cite This: *ACS Appl. Nano Mater.* 2023, 6, 15896−15905

Read Online

ACCESS | Metrics & More | Article Recommendations | Supporting Information

ABSTRACT: Naturally occurring halloysite nanotubes (HNTs) have attracted significant scientific interest due to their multifunctional behavior and biocompatibility. However, the application of HNTs in photonics is still unexplored. Here, natural HNTs with different lengths and diameters have been employed as passive scatterers for the generation of random laser (RL) emission from rhodamine B (RhB) in a colloidal phase. Upon pumping at 532 nm, mixed HNT-RhB disordered colloidal systems are shown to yield orange RL emission with a linewidth as small as ∼4 nm. Moreover, a statistical analysis of shot-to-shot correlations among RL modes reveals an obvious photonic paramagnetic to spin-glass transition with increasing pump energy, which is a unique statistical fingerprint of RL. Interestingly, besides acting as scatterers, the HNTs are also found to improve the photostability of RhB molecules. Indeed, HNTs help to better dissipate the excess energy deposited in the gain medium, thus protecting the dye from photodegradation and facilitating the achievement of RL. The results contribute to the theoretical understanding and technical development of low-cost RL devices based on widely available sources in view of multiple prospective applications in photonics.

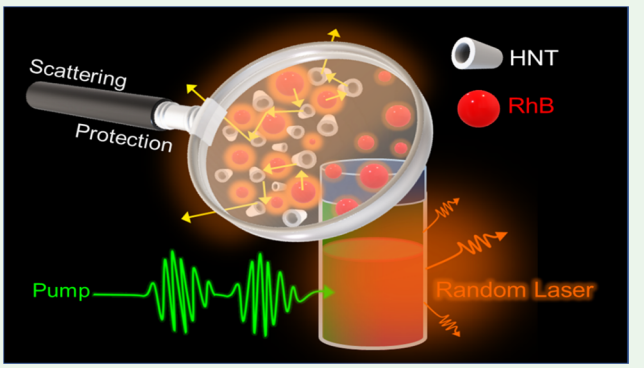

KEYWORDS: *halloysite nanotubes, light scattering, random laser, photostability, replica symmetry breaking*

1. INTRODUCTION

Nature is a treasury of multifunctional materials with exotic structures and amazing physical properties. For example, recent works have demonstrated a wide variety of two-dimensional (2D) materials exfoliated from different natural sources[1−4] and their energy harvesting applications. Also, one can utilize nature not only as a resource for synthesizing new materials but also as a source of some pre-existing nanostructures, as increasingly often reported in the literature.[5,6] Halloysite nanotubes (HNTs) are one such naturally occurring nanomaterial, whose surface chemistry and morphological properties are very attractive for many applications.[7,8] Generally, HNTs are hollow tubular shaped nanostructures of length in the micrometer range, consisting of aluminosilicate spiral layers with variable interlayer distances (∼0.6−1.0 nm) and variable inner and outer diameters ranging between ∼60−300 and ∼10−60 nm, respectively.[7] The basic unit cell formula of HNTs is $Al_2Si_2O_5(OH)_4{\cdot}nH_2O$, although a certain variability in structural features and precise chemical content is observed, depending upon the geological origin.[9−11] The high aspect ratio, hollow cavity, easy dispersibility, and stability of HNTs have diversified their applications starting from food packaging[10,12,13] to drug delivery[14−17] and catalysis.[18,19]

Only a few recent papers have explored so far the possible applications of HNTs in photonics and spectroscopy.[20,21] Among these, the immobilization of metal nanoparticles over the external surface of HNTs results in better surface-enhanced Raman scattering,[22] and second harmonic generation from HNTs under 800 nm femtosecond laser radiation has been recently demonstrated by Fidecka et al., paving the way to bioimaging applications.[23] Interestingly, due to their relatively large sizes in the order of hundreds of nm, HNTs are rather strong light scatterers despite the refractive index of halloysite materials (1.54)[24] being lower than other common scatterers such as TiO_2 (2.5−2.8). This property, combined with very high colloidal stability and the large specific surface available for dye adsorption, makes them quite promising as scattering media for random lasing (RL) applications. Indeed, the use of 2D kaolinite, a sheetlike hydrous silicate closely related to

Received: June 22, 2023
Accepted: August 21, 2023
Published: August 30, 2023

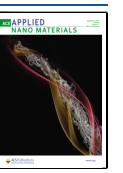

HNTs, as a passive scatterer for random laser (RL) emission from organic dye was reported in a recent work.[25]

Since its first invention in 1960, the laser is one of the most important and versatile sources of light in current technology. However, the use of lasers in imaging is sometimes limited by their high spatial coherence, as they cause speckle patterns. Moreover, the use of conventional lasers in some applications is somewhat limited by their bulky nature, high cost, and high output energy. In contrast, optical feedback offered by an active disordered medium can lead to adequate photon amplification for generating laser emission from a mirrorless open system, which is known as random laser (RL).[26] RLs can be designed by a suitable mixture of traditional gain molecules with a disordered nanosystem acting as a scatterer. The interest in RL has skyrocketed in the last few years: RLs have emerged as a viable alternative to traditional lasers, providing a source of light with high intensity and monochromaticity but lower coherence, very low cost, and ease of fabrication. A wide range of nanosystems such as semiconductor nanoparticles,[27] quantum dots,[28] polymers,[29] and 2D materials[30] have been employed as passive and active scatterers for RL action. Recent research has revealed many benefits of RLs such as low spatial coherence,[31] bichromatic emission,[32,33] and multiphoton excitation,[34] leading to many possible uses[26] in speckle-free imaging, theranostics, anticounterfeiting, and sensing.

Besides possible applications, RLs have also attracted a large theoretical interest as a photonic model to study the physical properties of disordered complex systems.[35] In particular, Ghofraniha et al. have utilized RL emission to gain the first experimental verification of spin-glass theory (SGT), one of the leading paradigms to describe the physical behavior of complex systems.[36] This first observation has triggered a very large interest in RLs in the community working in this area. Thereafter, a number of research groups have tested SGT in different RL systems through the observation of so-called, replica symmetric breaking (RSB),[37−39] which is a characteristic statistical behavior of the shot-to-shot laser fluctuations of a complex disordered system such as RL.

Most RSB studies of RL are conducted in high-viscosity media or a solid polymer matrix because the observation of RSB is made impossible by the diffusion of scatterers and dyes over time. For example, the RhB-TiO_2 disordered system, one of the archetypal systems displaying RL,[40] fails to exhibit RSB[34] even when dispersed in highly viscous ethylene glycol (EG). On the other hand, stopping dye diffusion tends to enhance photobleaching effects. Even in conventional laser dyes, photobleaching is often observed under prolonged pumping due to poor thermal conductivity and diffusivity of the dispersing medium.[41] Similarly, strong photobleaching of dye molecules in the presence of scatterers is one of the practical drawbacks of RLs in terms of long-term applications. Actually, good chemical compatibility among the organic dye gain molecule and the scatterer is required to achieve high photostability, especially in a low-viscous colloidal system.[35,36] Interestingly, some works have found that dye photobleaching in EG can be prevented by the addition of suitable nanoparticles.[41,42]

Overall, comprehensive research is still needed to design multifunctional scatterers for RL emission, which both have high scattering efficiency and grant high resistance to photobleaching to the gain molecules in a colloidal medium, while, from a fundamental point of view, the studies of RSB in colloidal-based RLs remain scanty.[35,43] Herein, we have employed, for the first time, two natural HNT samples collected from different geological deposits as passive scatterers to generate RL emission without any cavity feedback when combined with rhodamine B (RhB) dye. The designed HNT-RhB colloidal media yield incoherent RL emission peaking at ∼591 nm with a more than 10-fold narrowing with respect to RhB fluorescence. The abrupt reduction in emission lifetime with an increase in input pump energy provides further strong evidence of lasing behavior. Interestingly, we find that HNTs behave as photostabilizers of dye molecules in highly viscous base media, *i.e.*, poly(ethylene glycol), as they can act as thermal conductivity boosters.[44] Indeed, HNTs not only act as passive scatterers for RL but also as a bodyguard for RhB molecules, greatly increasing their resistance to photobleaching upon prolonged pumping. Thereby, HNT-RhB composites are particularly promising as quasi-monochromatic RL light sources with long-term stability. In addition, HNT-RhB suspensions are shown to provide a suitable platform for the verification of theoretical photonic spin-glass transition (SGT), as we demonstrate by providing clear experimental evidence of the typical RSB behavior in the RL emission.

2. EXPERIMENTAL SECTION

2.1. Halloysite Nanotubes (HNTs). Both of the HNT samples were obtained from natural sources. The halloysite sample named HNT1 was supplied by I-Minerals Inc., and it was obtained from the Latah County deposit in NW Idaho, North America.[45] HNT1 consists of halloysite nanotubes for at least ∼90% in weight.[45] The halloysite sample named HNT2 was collected from Jarrahdale (Western Australia) from a deeply weathered profile in dolerite, exposed in a railway cutting. The mineralogy of the site and the main characteristics of HNT2 have been reported in the literature.[9] As HNT2 was formed as a consequence of *in situ* weathering of aluminosilicate minerals, it had a relatively high level (*ca.* 20%) of other components such as fine-grained quartz, anatase, mica, iron oxides, and feldspar. Prior to their use in further experiments, both HNT1 and HNT2 have been rinsed with deionized water 5 times and dried out under a vacuum for 48 h.

2.2. Characterization of HNTs. ζ-potential and dynamic light scattering (DLS) measurements were carried out using a ζ-sizer Nano-ZS (Malvern Instruments) equipped with a He−Ne laser (λ = 632.8 nm). For ζ-potential experiments, disposable folded capillary cells were used. Electrophoretic mobility was obtained by measuring the velocity of the particles in an electric field by using laser Doppler velocimetry and phase analysis light scattering. The scattering angle was set at 12.8°, while the temperature was fixed at 25.0 ± 0.1 °C. The Smoluchowski approximation was used to calculate the ζ-potential as it is considered a good approximation for particles larger than 0.2 μm in water. All experiments were performed in triplicate, and average values were provided. Regarding DLS measurements, the field-time autocorrelation functions were analyzed through inversion of the Laplace transform (ILT), allowing us to obtain the distribution (expressed in terms of number density) of the hydrodynamic diameters of halloysite nanotubes. X-ray fluorescence (XRF) measurements have been carried out by means of an Olympus Analyzer (Delta series) with a 4 W X-ray source. HNT powder was pressed under 8×10^3 kg cm^{-2} for 10 min to obtain a tablet for the measurement.

2.3. Steady-State Optical Measurements. Optical extinction spectra of RhB and HNT suspensions were measured in 1 cm cuvettes by using an Avantes, Star Line ULS2048CLEVO optical fiber spectrometer working in the range 200−1300 nm, using a dual deuterium/halogen lamp as a broadband light source. Steady-state photoluminescence (PL) emission spectra and PL quantum yield (PLQY) of RhB solutions were measured on the same spectrometer while exciting the samples by a laser diode at 532 nm. Emission spectra were collected perpendicularly to the direction of the

https://doi.org/10.1021/acsanm.3c02840
ACS Appl. Nano Mater. 2023, 6, 15896−15905

incoming excitation beam. To estimate PLQY, we made use of an integrating sphere (Labsphere 3PGPS053SL) internally covered by Spectralon. The PLQY was calculated *via* the following formula: PLQY = $I_S/(S_r - S_S)$, where I_S refers to the spectrally integrated photoluminescence of the sample and S_r and S_S are the spectrally integrated scattering signal around the excitation wavelength of, respectively, the reference (water) and the sample, *i.e.*, an aqueous solution of RhB.

2.4. Preparation of an Active Medium for the RL Experiment. First, rhodamine B dye (RhB, Sigma-Aldrich) was dissolved in 5 mL of deionized (DI) water to get a homogeneous solution. In our RL experiment, we used two different types of HNT samples, namely, HNT1 and HNT2 as passive scatterers. Therefore, the starting solution of RhB dye was separately mixed with an aqueous dispersion of HNT1 and HNT2. Henceforth, the colloidal RL media consisting of RhB combined with HNT1 (HNT2) are designated as HNT1-RhB (HNT2-RhB). In these samples, the concentrations of RhB and HNTs are 100 μM and 0.02 wt %, respectively. Similarly, we also prepared similar homogeneous dispersions of bare RhB and HNT-RhB mixtures in 95 v/v% poly(ethylene glycol) (PEG) to test the viability of the RSB principle in RL emission.

2.5. RL Experiment. A Q-Switched neodymium-doped yttrium aluminum garnet (Nd:YAG) laser (Quanta system, SYL-201) at 532 nm (2nd harmonic of 1064 nm) having a pulse duration of 5 ns and 10 Hz repetition rate was used for optical pumping. A detailed schematic of the experimental setup for measuring RL emission is shown in Figure S1. The pump beam is first passed through an aperture of diameter 4 mm and then focused to the sample position by use of a plano-convex cylindrical lens (f = 15 cm). The active RL medium is placed in a cylindrical glass cuvette with a 15 mm outer diameter, positioned slightly away from the focal point of the lens, with the excitation beam hitting the cuvette perpendicularly to the outer surface. In this geometry, we estimate the vertical width of the excitation line on the surface of the sample to be about 0.15 mm. Using a cylindrical (as opposed to square) cuvette allows for eliminating Fabry−Perot cavity effects[46] due to reflections from cuvette wall, in order to single out the effects of RL. The emission from the excited sample was collected by an optical fiber (numerical aperture 0.22) positioned ∼5 cm away from the sample cuvette.

During the first explorative phase of the experiment, we tested the spectral characteristics of the emission at several angles from the pumping beam. We typically found much more pronounced narrowing in the forward direction (transmission mode) as compared to the backward direction (reflection mode). We believe this to be a combined effect of the geometry of the gain region and the cylindrical geometry of the vial, which strongly favors amplification along the forward propagation direction of the pumping beam. For this reason, we mainly conducted the measurements in transmission mode. Specifically, the RL spectra shown in the rest of the paper were collected at 45° from the forward direction of the pump beam (see Figure S1) using an optical fiber. The optical fiber was finally connected to a spectrometer (Thorlabs, CCS200, <2 nm spectral resolution) for spectral analysis of the emitted light. Each emission spectrum shown in this work was extracted by averaging 1000 pulse shots. A digital photograph of the colloidal RL system inside a cylindrical cuvette and in operating condition is shown in the inset of Figure 2b. Finally, fluorescence decay kinetics of the RhB dye with and without HNT scatterers was measured using an intensified CCD camera (PI-MAX Princeton Instruments, Trenton, NJ) synchronized to the pump source, *i.e.*, the Q-Switched Nd:YAG laser. Data acquisition consists of recording the emission spectra by integrating the signal over a certain temporal window at different programmable delays from photoexcitation in order to reconstruct the kinetics of the entire decaying emission band.

3. RESULTS AND DISCUSSION

3.1. Structural and Optical Properties of the HNT Scatterers and Gain Media. A general structural and chemical composition of HNT is schematically shown in Figure 1a. The morphology of the two samples of halloysite nanotubes (HNTs) was assessed by means of field-emission

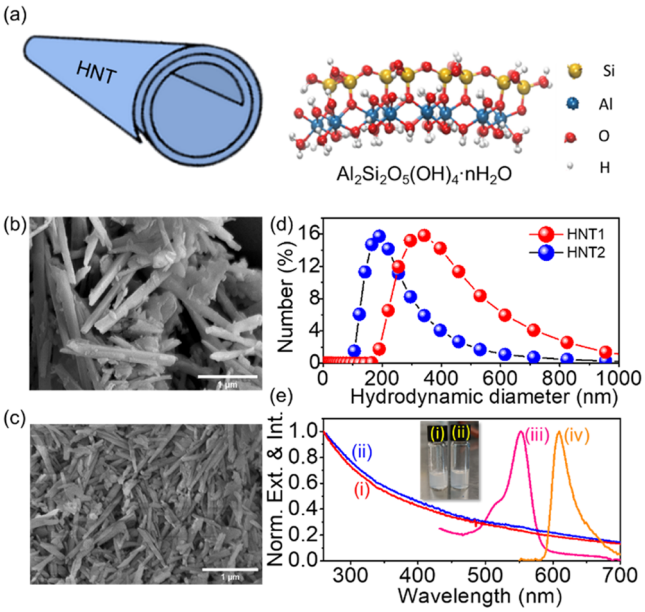

Figure 1. Structural and optical characteristics of the scatterer and the gain medium. (a) Schematic of HNT depicting its structure and chemical composition. FESEM images of (b) HNT1 and (c) HNT2. (d) Number density distribution of the hydrodynamic diameters obtained by DLS experiments performed on 0.02 wt % HNT1 and HNT2 dispersions in water. (e) UV−vis extinction spectra of (i) HNT1, (ii) HNT2, both dominated by scattering contributions, and (iii) RhB dye. (iv) PL emission intensity (l_{ex} = 532 nm) of RhB dye.

scanning electron measurements (FESEM), shown in panels (b) and (c) of Figure 1. The images clearly reveal the tubular shape of the HNTs and the large polydispersity of both HNTs obtained from North America (hereafter called HNT1) and HNTs obtained from Australia (HNT2). It can also be noted that HNT1 (Figure 1b) is composed of larger nanotubes than HNT2 (Figure 1c).

From DLS experiments (Figure 1d) conducted at a concentration of 0.02 wt %, the samples show different average hydrodynamic diameters (330 and 190 nm for HNT1 and HNT2, respectively), consistent with the different sizes highlighted by SEM. The displayed distribution of hydrodynamic diameter is monomodal, albeit very broad. Nevertheless, DLS results indicate that the diffusion of both HNTs in water is consistent with that of single clay nanotubes[47] avoiding the formation of clusters in the investigated dispersions. As concerns the surface charge, both halloysite nanotubes possess similar characteristics, as evidenced by their ζ-potential values, which were found to be −23.1 ± 0.4 (HNT1) and −25.8 ± 0.7 mV (HNT2), guaranteeing a relatively high colloidal stability. The relatively large size, leading to predictably strong scattering, and the relatively high colloidal stability of HNTs, as expected from the large ζ-potential values, make them good candidates to be passive light scattering elements in the generation of random lasing emissions from dye molecules. Finally, chemical analysis of the HNT samples was carried out by XRF (Table S1). XRF reveals that the composition of the major oxides agrees with the high proportion of kaolin group mineral (SiO_2 ∼ 46.5%, Al_2O_3 ∼ 39.5%) in both HNT samples, although HNT2

https://doi.org/10.1021/acsanm.3c02840
ACS Appl. Nano Mater. 2023, 6, 15896−15905

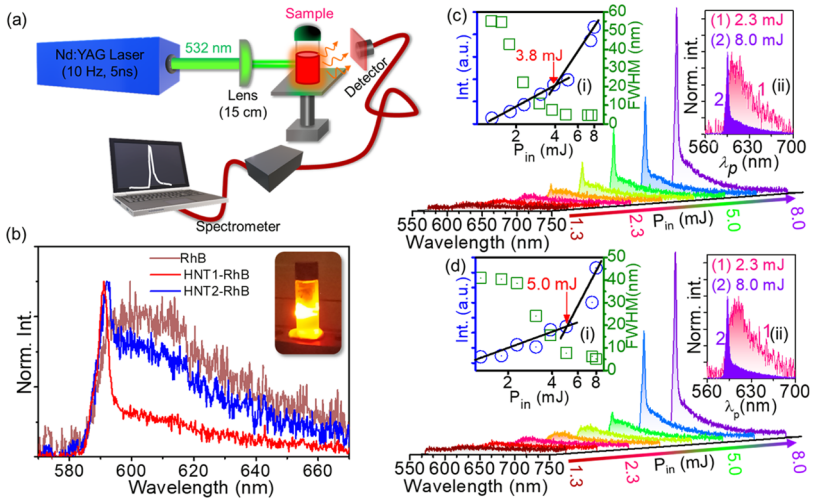

Figure 2. RL experiment in an aqueous mixture of RhB and HNTs. (a) Schematic illustration depicting the RL experiment setup. (b) Normalized emission spectrum of RhB, HNT1-RhB, and HNT2-RhB excited by 532 nm laser pulses at P_{in} = 5.0 mJ/pulse. Inset: the digital photograph of the HNT1-RhB RL system in operating conditions. P_{in}-dependent emission spectra of (c) HNT1-RhB and (d) HNT2-RhB; insets: (i) variation of output emission intensity and FWHM with P_{in} and (ii) normalized emission spectra at P_{in} below and above P_{in}^{Th}.

possesses a higher SiO_2 content due to the presence of fine-grained silica impurities. In contrast, the HNT2 sample contains larger amounts of TiO_2 and Fe_2O_3 compared with those of HNT1. These results are consistent with literature data reported by Pasbakhsh et al.[9]

The optical properties of the gain and scattering media tested for RL emission are summarized in Figure 1e. When measuring the extinction spectra of both HNT samples in a spectrophotometer, we see an unstructured spectral profile overwhelmingly dominated by scattering in the entire UV−vis spectral range. Notably, HNTs do not show any defined optical absorption around 532 nm, which is the pump laser wavelength used for the random lasing experiments, or in the emission range ($\lambda \geq 600$ nm) of the active medium we chose for these experiments, *i.e.*, RhB molecules. However, any minor absorption bands of HNTs in these regions might be concealed under the overwhelming scattering contributions. Anyway, natural, unprocessed HNT samples overall appear to be promising candidates to act as passive scatterers to assist RL emission by photoexciting RhB molecules under a 532 nm pump laser beam. In Figure 1e, we also report the normalized extinction and emission (λ_{ex} = 532 nm) spectra of RhB. While the $\pi \rightarrow \pi^*$ absorption[48] peaks at 553.0 ± 0.5 nm, the visible PL emission peaks at 608.0 ± 0.5 nm, with a large Stokes shift from absorption maxima that guarantees a very low possibility of loss of the PL emission due to reabsorption. The PLQY of RhB in the absence and presence of HNTs (0.02 wt %) was measured to be 0.31 and 0.27, respectively, hence ruling out any substantial quenching effect of the dye by HNTs.

3.2. Random Lasing in the Presence of HNT Scatterers. On these grounds, we prepared a colloidal mixture of HNTs and RhB dye to be tested for RL emission under 532 nm pulse laser excitation (Figure 2a). Figure 2b depicts the emission profile of the active medium, *i.e.*, RhB dye, suspended in water at a concentration of 100 mM, without and with the HNT scatterers, collected at an excitation pump energy (P_{in}) of 5.0 mJ/pulse. Upon this condition, the emission profile of the bare RhB consists of a broad spontaneous emission band centered at ∼600 nm (dark red spectrum in Figure 2b). In comparison, when we prepare a mixed solution of 100 mM RhB dye with HNTs (0.02 wt %), the latter act as scatterers, triggering the onset of RL (blue and red spectra in Figure 2b). This can be appreciated by the appearance of a narrow peak at 591 ± 1 nm, especially evident for HNT1-RhB (Figure 2b). Only when the pumping intensity is further increased (8.0 mJ/pulse), we observe the appearance of a sharp peak at 587 ± 1 nm also for bare RhB (Figure S2), which is due to amplified stimulated emission, but such a narrow peak coexists with a broad spontaneous emission background of comparable intensity (Figure S2). In contrast, the addition of HNT (0.02 wt %) scatterers leads to the almost complete suppression of the broad fluorescence in favor of the narrow RL peak (Figure S2). Figure 2c,d reports the emission profiles of HNT1-RhB and HNT2-RhB as recorded at different P_{in}. For both of the systems, the progressive appearance of the sharp RL peak at ∼591 nm is obvious with increasing pumping power, while two key characteristics of RL emission[49,50] are clearly identifiable (insets (i) and (ii) of Figure 2c,d): the change of the slope in the dependence of the emission intensity *vs* P_{in} and the onset of spectral narrowing, both observed after a threshold pumping power. The threshold pumping energy (P_{in}^{Th}) for triggering the onset of RL is found to be ∼3.8 and 5.0 mJ/pulse for HNT1-RhB and HNT2-RhB, respectively. From Figure 2c,d, the emission FWHM is reduced down to ∼4.7 nm for HNT-RhB systems. Unlike the HNT-RhB systems, such a strong spectral narrowing with an increase in P_{in} is not observed for a bare dye solution (Figure S3). As already mentioned, in this case, the narrow peak due to amplified spontaneous emission is only observed at the highest excitation power and always coexists with a strong and broad fluorescence background. Therefore, the scattering from HNT is crucial in achieving a strong spectral narrowing, which is a key feature of RL. As shown in Figure S4, we repeated these experiments at variable concentrations of scatterers. A similar kind of behavior is also observed when the experiment is performed at 0.01 and 0.03 wt % scatterers, as shown in Figure S4. The P_{in}^{Th} and the spectral linewidth are found to reach a minimum at a scatterer concentration of 0.02 wt % for both HNTs, which is therefore optimal to achieve RL conditions.

https://doi.org/10.1021/acsanm.3c02840
ACS Appl. Nano Mater. 2023, 6, 15896−15905

Apart from spectral narrowing and a change of the slope in the growth of emission intensity, the onset of RL should also lead to a reduction of the decay lifetime due to the contribution of stimulated emission to excited-state depopulation. To check this aspect, we have measured the time-resolved photoluminescence spectra of HNT1-RhB at P_{in} = 1.5 and 7.5 mJ/pulse (Figure 3), which is below and above the

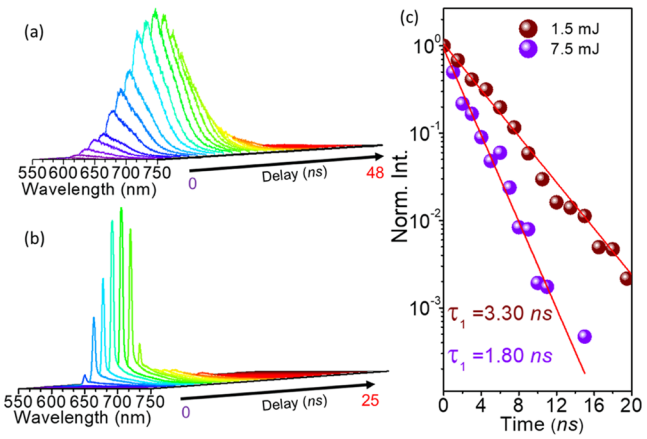

Figure 3. Time-resolved emission characteristic of the HNT-based RL system. Time-resolved photoluminescence of the HNT1-RhB system at P_{in} = (a) 1.5 and (b) 7.5 mJ/pulse. (c) Normalized emission decay profile, as isolated from the decaying portion of the data in panels (a, b), and respective least-squares fitting curves at P_{in} = 1.5 and 7.5 mJ/pulse.

P_{in}^{Th} value, respectively. Below the P_{in}^{Th}, we detected the standard lifetime of RhB in a water solution (Figure 3a): τ = 3.3 ± 0.2 ns, occurring without any spectral evolution during time. When we photoexcite the HNT-RhB system above the lasing threshold, the lifetime of this peak is 1.8 ± 0.2 ns. Therefore, this is shorter than the standard spontaneous emission lifetime photoexcited at low power. Such an effect is indeed expected due to the additional contribution of stimulated emission, and thus laser amplification, to the depopulation rate of the excited state. This result confirms again the onset of RL above the threshold pumping intensity.[30,51]

From a practical point of view, one key problem of many colloidal organic RLs is their poor photostability under continuous operation.[43] Chemical incompatibility among the organic gain molecule and the scatterer may be responsible for this. For example, semiconductor nanoparticles such as TiO_2 nanoparticles (rutile), when used as scatterers, may cause the photodegradation of organic dye molecules under 532 nm pulsed laser pumping.[35] Therefore, a careful choice of the scatterer for stable RL emission from organic dye is fundamental, while this issue often represents one of the limiting factors in the practical applications of RL.

For these reasons, we have tested the photostability of RhB emission, with and without HNT scatterers, under continuous pumping with the intensity of P_{in} = 8.0 mJ/pulse, which is well above the RL threshold for HNT-RhB. These experiments were carried out both in water and in a highly viscous solvent (PEG). Testing photostability in a highly viscous environment is important both from a practical viewpoint, *e.g.*, for perspective applications of these nanocomposites in a solid-state device, and in order to test the RL system for the occurrence of RSB effects (*vide infra*). Indeed, photodegradation in PEG may be potentially much faster than in DI water due to the absence of diffusion.

The results of these photostability tests are shown in Figure 4a. In the case of an aqueous solution, we see RhB emission to

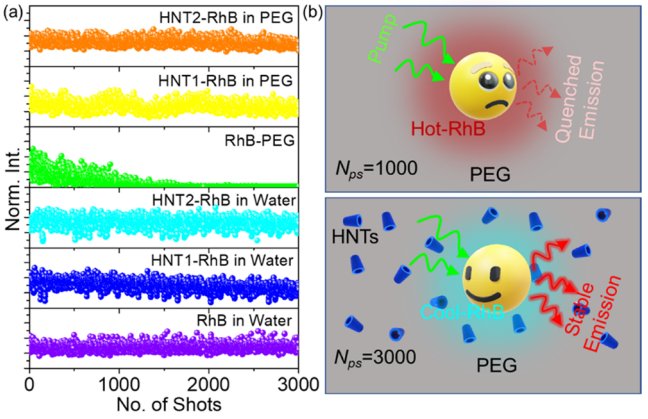

Figure 4. Stability of the HNT-RhB system in different base solvents. (a) Normalized peak emission intensity as a function of the number of shots N_{ps} for bare RhB and HNT-RhB systems dispersed in DI water and PEG as base solvents, as obtained from measurements performed at a 10 Hz pumping laser repetition rate and P_{in} = 8 mJ/pulse (well above threshold). (b) Cartoon representation depicting the role of HNTs in protecting the emission of RhB in PEG.

be quite stable under high-intensity 532 nm pumping. As seen from the data, the addition of the scatterers does not lead to any detrimental effects, as we found HNT1-RhB and HNT2-RhB to be as stable as bare RhB upon the same testing conditions. The absence of photobleaching effects for these aqueous solutions is most likely due to the ability of the emitters to quickly diffuse in and out of the illuminated volume. The results are very different in PEG. Unsurprisingly, we now observe strong photodegradation of bare RhB as a consequence of reduced diffusion, leading to the complete disappearance of the emission within a thousand shots. However, an interesting result is obtained when adding HNTs. In fact, we observe that RhB photostability in PEG is drastically improved in the presence of HNT scatterers, where no photodegradation is observed (see Figure 4a). Thus, HNTs are not only capable of acting as passive scatterers to generate RL emission from RhB but also offer a protection effect to the dye against photodegradation, which more than balances the effects of reduced viscosity in a highly viscous environment. In addition, RL emission of HNT1-RhB and HNT2-RhB suspended in PEG is found to be even more efficient than water, with a reduction of threshold down to 1.80 and 3.20 mJ/pulse, respectively (Figure S5).

We propose that such a protective effect of HNT against photodegradation is due to the enhanced thermal diffusion of the medium upon the addition of the scatterers, which should help to dissipate the excess energy deposited at the gain medium through intense photoexcitation, thus protecting the dye from degrading under continuous operation of RL. In fact, it has been reported that thermal conductivity k of PEG can be improved by the addition of nanoparticles,[52,53] and as much as an ∼88.6% enhancement in the k value of PEG in the presence of HNTs was recently observed[44] (relevant literature data are summarized in Figure S6). Therefore, the presence of HNTs in a PEG solution enhances the photostability of RhB molecules

https://doi.org/10.1021/acsanm.3c02840
ACS Appl. Nano Mater. 2023, 6, 15896−15905

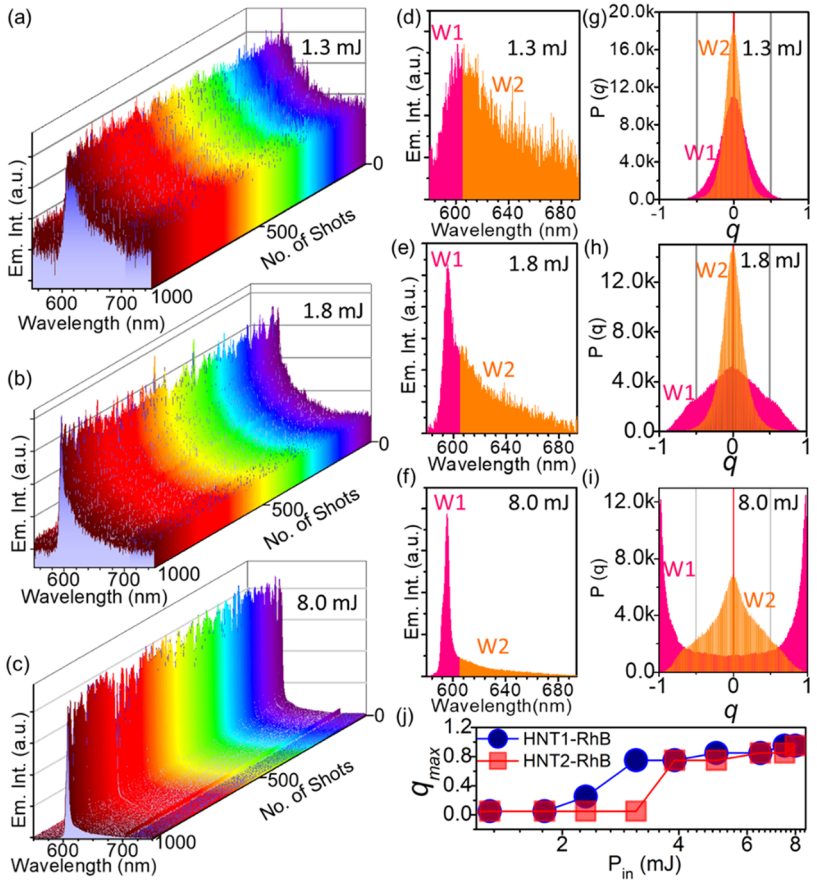

Figure 5. Replica symmetry breaking of the HNT1-RhB RL system in PEG ($P_{in}^{Th} \sim 1.8$ mJ). (a–c) Pulse-to-pulse fluctuations for 1000 emitted spectra of the HNT1-RhB RL system. (d–f) Averaged emission spectra at different P_{in} are shown to identify the spectral window, where RL (W_1, pink) and spontaneous emission (W_2, orange) are observed. (g–i) Distribution function $P(q)$ of HNT1-RhB RL computed for spectral windows W_1 (pink) and W_2 (orange) at three different P_{in}. (j) Variation of q_{max} with P_{in} for two different disordered systems.

during lasing operation,[41] as schematically depicted in Figure 4b, also leading to increased RL performance in the highly viscous medium (Figure S5). It is worth noting that the P_{in} used in our experiment is high, similar to some of the previous studies on RL.[35,36,43] It is the very good photostability and resistance to laser heating of our emitters, as obvious from the data in Figure 4, that conveniently allows us to use such high pumping powers without observing any significant photobleaching. In perspective, such remarkable stability may even make it possible to achieve RL from HNT-RhB under continuous-wave pumping.

To learn more about the conditions in which RL is achieved in the HNT-RhB composites, it is instructive to estimate the characteristic length scales at play here. Theoretically, the phenomenon of RL in a gain region of size L is controlled by the inter-relation among the average gain length $l_g = 1/N_g\sigma_e$ and the average scattering length $l_{sc} = 1/N_{sc}\sigma_{sc}$,[50,54] where N_{sc} (N_g) is the number density of scatterers (gain molecules), σ_{sc} is the scattering cross section of the scatterer, and σ_e is the stimulated emission cross section of the gain molecules. On the one hand, the gain length should be smaller than the scattering length in order to have efficient RL amplification. Furthermore, depending on the relation between the gain (l_g) and scattering (l_{sc}) spatial scales, RL can occur either as a diffusive, incoherent process ($\lambda < l_{sc} < L$) or as a coherent process ($l_{sc} \sim \lambda$), made possible by the formation of transient "loop" microcavities acting as optical resonators.

In our case, the value of σ_e for RhB molecules is estimated from the following relation

$$\sigma_e(\lambda) = \frac{\lambda_e^4 E_0(\lambda)}{8\pi c n^2 \tau} \quad (1)$$

where $E_0(\lambda)$ is the normalized emission profile, τ is the radiative lifetime, c is the speed of light, and n is the refractive index of the surrounding medium (water). The radiative lifetime can be estimated from the measured lifetime and quantum yield (PLQY) as $\tau = \tau_0/\text{PLQY} \sim 3.30$ ns/0.27 = 12.1 ns. From this, one can calculate $\sigma_e \sim 1.4 \times 10^{-16}$ cm^2, leading to a value of $l_g \sim 0.12$ cm at our concentration of dye molecules, $N_g = 6 \times 10^{16}$ mL^{-1}. From the extinction spectra in Figure S7b, the values of l_{sc} at the emission peak wavelength for HNT1 (HNT2) are estimated to be ~0.40 (0.32) cm, as the inverse of the measured extinction coefficient (assuming all extinction is due to scattering). Therefore, the condition of adequate photon amplification for RL emission,[50] which is $l_{sc} \geq l_g$, is satisfied. Furthermore, considering the typical size of the gain region, $L \sim 1$ cm, and an RL wavelength of $\lambda = 591$ nm, the photon transport within a random medium containing RhB and HNTs occurs in the diffusive or incoherent regime ($\lambda < l_{sc} < L$). RL emission performance of HNT1 and HNT2 is expected to be identical because of their similar linear optical properties around ~600 nm. Anyway, inhomogeneity in the distribution of the scatterer may lead to a slight improvement in the P_{in}^{Th},[55−57] as we have observed for HNT1-RhB.

https://doi.org/10.1021/acsanm.3c02840
ACS Appl. Nano Mater. 2023, 6, 15896−15905

3.3. Photonic Paramagnetic to Spin Glass Transition in HNT-Based Random Laser. As a final goal of this work, we validated the observation of random lasing in HNT-RhB through a study of shot-to-shot RL intensity fluctuations aimed at highlighting the phenomenon of replica symmetry breaking (RSB).[36] RSB is a concept originally formulated in the context of spin glass theory.[58] It is associated with the fact that identical copies (replicas) of a disordered system under identical experimental conditions, such as an RL emitting a sequence of laser shots, can explore different equilibrium configurations. The occurrence of RSB in RLs was only proven experimentally a few years ago[36] and has inspired intense research motivated by the related conceptual implications for the photonics of random systems. From another viewpoint, the analysis of RSB is a key factor in validating the observation of RL from the analysis of the nature of the randomness of a disordered gain medium pumped above the threshold.

Here, we experimentally investigated the RSB phase transition by analyzing the statistics of shot-to-shot spectral intensity fluctuations in our system. A necessary condition to perform this study is that the spatial distribution of scatterers does not change from shot to shot, generating identical "replicas" of a specific configuration of the disordered system. As a consequence, low-viscosity solvents are avoided for inspection of RSB in RLs due to the changes with time caused by Brownian motion or fast precipitation of scatterers.[35] Hence, high-viscous solvents or polymer matrix is preferable for such studies.[36,58] In our case, we conducted our experiments on HNT-RhB in PEG, showing high stability and efficiency as demonstrated above.

To fulfill our aims, we recorded three sets of N_{ps} = 1000 single-shot RL emission spectra, as shown in Figure 5a−c, below and above the lasing threshold. For each set acquired at a fixed power, each shot of the pumping laser generates a replica output spectrum, as it is produced under identical experimental conditions. The fluctuation in intensity $\Delta_i(l_k)$ of the spectrum I = 1,2,⋯,N_{ps} at a particular wavelength can be expressed as $\Delta_i(l_k) = I_i(l_k) - I_{av}(l_k)$, where $I_{av}(l_k)$ represents the averaged intensity at l_k over the N_{ps} shots. Now, a pulse-to-pulse intensity correlation function or q_{ij} can be calculated from the data as[35]

$$q_{ij} = \frac{\sum_{k=1}^{N} \Delta_i(\lambda_k)\Delta_j(\lambda_k)}{\sqrt{\sum_{k=1}^{N} \Delta_i^2(\lambda_k)}\sqrt{\sum_{\lambda_k=1}^{N} \Delta_j^2(\lambda_k)}} \quad (2)$$

where i,j = 1,2,⋯,N_{ps} denote the replica labels and N represents the total number of sampled wavelength points. The quantities q_{ij}, ranging from −1 to 1, can be taken as a measure of the overlap between pulse-to-pulse intensity fluctuations. The onset of RSB can then be highlighted by the change of the shape of the statistical distribution $P(q)$ of this so-called order parameter q. In particular, to better disentangle RL emission from the spontaneous emission background, we performed our calculations of $P(q)$ in two different spectral windows, as shown in Figure 5d−f: (i) ∼588 to 616 nm (W_1) and (ii) 617 to 706 nm (W_2). Figure 5g−i displays the distributions $P(q)$ found at various pumping powers for the HNT1-RhB system. Similar plots for HNT2-RhB are shown in Figure S8.

Clearly, the statistical distribution $P(q)$ always has a maximum at q_{max} = 0 when the calculation is performed within W_2. Similarly, within W_1, the probability distribution function $P(q)$ shows a maximum at q_{max} = 0 when the system is pumped well below the threshold. This observation signifies the independent fluctuation of uncorrelated photonic modes below the threshold.[35] In this regime, the distribution functions $P(q)$ calculated within W_1 and W_2 are almost identical (Figure 5g), and no RSB is observed. However, the shape of $P(q)$ within W_1 changes with further increasing of P_{in} and finally shows clear maxima at $q_{max} = \pm 1$ when the system is pumped well above P_{in}^{Th} (Figure 5i). This is the key fingerprint of RSB, indicating that the disordered system begins to operate in the photonic analogue of a glassy phase. In this regime, the intensity fluctuations on the many different photonic modes contributing to RL are correlated with each other. Such a behavior is characteristic of RL,[35,59] and is not observed for fluorescence emission and traditional lasers.[36] For instance, we have also computed the probability distribution function of the RhB emission at P_{in} = 8.0 mJ/ pulse and pump laser beam in Figure S9, observing a maximum at q_{max} = 0 for both cases, with no evidence of RSB. The variation of q_{max} with P_{in} for different HNT-RhB is presented in Figure 5j. Both the HNT-based RL systems exhibit a similar transition but at different P_{in}. Notably, P_{in} at which q_{max} flips from 0 to 1 is nearly equal to the P_{in}^{Th} determined from their output *vs* input characteristics, as shown in the inset of Figure S5a,b. Therefore, the observation of a clear transition to an RSB regime above the threshold conclusively validates the attribution of the HNT-RhB emission to RL. Last but not least, we also show in Figure S10 the calculation of $P(q)$ over the entire spectral range (588−706) nm for comparison with the data shown in Figures 5 and S8, obtained by separating the W_1 and W_2 spectral windows. Even in Figure S10, we see a clear transition from spontaneous emission to random lasing, albeit RSB behavior is slightly less pronounced than in Figures 5 and S8, demonstrating that the residual contribution of fluorescence to the overall emission becomes negligible at high pumping energies.

4. CONCLUSIONS

We demonstrate the possibility of employing naturally occurring halloysite nanotubes as passive scatterers for generating RL emission in solution as well as an experimental platform for the verification of photonic spin glass theory in a colloidal disordered system. The quality of RL emission is found to be dependent on the size distribution and chemical composition of the scatterers.[59] In an aqueous medium, HNT-RhB nanocomposites provide an RL emission at ∼591 nm with a linewidth of ∼4 nm and a narrowing of more than 10 times with respect to fluorescence. Similar results are obtained in higher viscous solvents such as PEG. Interestingly, HNTs also display an ability to solve the problem of photobleaching of RhB emission in a highly viscous solvent, thanks to enhanced energy dissipation. Therefore, we are able to use the HNT-RhB colloidal disordered system to demonstrate the transition from fluorescent paramagnetic to RSB behavior, as predicted by spin glass theory.

The characteristics and performance of RL emission are comparable to the recently reported colloidal disordered system containing an artificially designed 2D material as passive scatterers, paving the way to multiple applications of HNT-based RLs, such as speckle-free imaging,[31] medical diagnostics, anticounterfeiting.[50,57] In addition, HNTs are a cheap and abundantly available nanomaterial suitable for a true mass-scale industrial application,[24] making them very appealing for applications. In fact, different deposits worldwide offer

https://doi.org/10.1021/acsanm.3c02840
ACS Appl. Nano Mater. 2023, 6, 15896−15905

HNTs with peculiar morphology, purity, and size distribution,[9] and compared to other nanotubular particles such as carbon nanotubes, for halloysite clay, the world supply is in the range of 50,000 tons/year.[24] In perspective, the anisotropic shape of HNTs, which are morphologically similar to nanowires and nanotubes, may pave the way for further developments. For instance, the difference in absorbance and scattering for light impinging on the nanowires in longitudinal versus transverse orientations may be beneficial for offering tunable RL emission. Moreover, the formation of a cylindrical waveguiding structure may lead to mode-selective RL emission, an effect that cannot be achieved by spherically shaped scatterers. Therefore, our results pave the way to use natural HNTs as highly efficient natural nanomaterials for a wide range of photonic applications.

■ ASSOCIATED CONTENT

Supporting Information

The Supporting Information is available free of charge at https://pubs.acs.org/doi/10.1021/acsanm.3c02840.

> Pump power (P_{in})-dependent emission spectra of bare RhB dye, P_{in}-dependent emission spectrum of the HNT1-RhB aqueous system containing different amounts of HNT1 scatterers, RL emission behavior of HNT1-RhB in PEG, comparison of thermal conductivity of PEG without and with different nanoparticles, emission cross-sectional profile of RhB and extinction spectra of HNT1 and HNT2 (0.02 w %), and additional data on the RSB behavior of HNT-RhB nanocomposites, bare RhB, and pump laser beam (PDF)

■ AUTHOR INFORMATION

Corresponding Author

Fabrizio Messina − *Dipartimento di Fisica e Chimica, Università degli Studi di Palermo, 90123 Palermo, Italy;* orcid.org/0000-0002-2130-0120; Email: fabrizio.messina@unipa.it

Authors

Ashim Pramanik − *Dipartimento di Fisica e Chimica, Università degli Studi di Palermo, 90123 Palermo, Italy*

Alice Sciortino − *Dipartimento di Fisica e Chimica, Università degli Studi di Palermo, 90123 Palermo, Italy;* orcid.org/0000-0001-8361-3002

Marco Reale − *Dipartimento di Fisica e Chimica, Università degli Studi di Palermo, 90123 Palermo, Italy*

Pooria Pasbakhsh − *School of Engineering, Monash University Malaysia, 47500 Subang Jaya, Selangor, Malaysia;* orcid.org/0000-0003-4771-9453

Giuseppe Cavallaro − *Dipartimento di Fisica e Chimica, Università degli Studi di Palermo, 90123 Palermo, Italy;* orcid.org/0000-0002-2145-0161

Marco Cannas − *Dipartimento di Fisica e Chimica, Università degli Studi di Palermo, 90123 Palermo, Italy*

Giuseppe Lazzara − *Dipartimento di Fisica e Chimica, Università degli Studi di Palermo, 90123 Palermo, Italy*

Complete contact information is available at: https://pubs.acs.org/10.1021/acsanm.3c02840

Author Contributions

This manuscript was written through the contributions of all authors. All authors have approved the final version of the manuscript.

Notes

The authors declare no competing financial interest.

■ ACKNOWLEDGMENTS

EU is acknowledged for financial support (CARLITO, Grant agreement ID: 101061538). A.S., G.C., M.C., G.L., and F.M. acknowledge FFR2022 and FFR2023 funds received from UNIPA to carry out this research.

■ REFERENCES

(1) Mahapatra, P. L.; Singh, A. K.; Tromer, R.; Karthik, R.; Ambresha, M.; Costin, G.; Lahiri, B.; Kundu, T. K.; Ajayan, P. M.; Altman, E. I.; Galvao, D. S.; Tiwary, C. S. Energy Harvesting using Two-dimensional (2D) d-silicates from Abundant Natural Minerals. *J. Mater. Chem. C* **2023**, *11*, 2098−2106.

(2) Mahapatra, P. L.; Tromer, R.; Pandey, P.; Costin, G.; Lahiri, B.; Chattopadhyay, K.; Ajayan, P. M.; Roy, A. K.; Galvao, D. S.; Kumbhakar, P.; Tiwary, C. S. Synthesis and Characterization of Biotene: A New 2D Natural Oxide from Biotite. *Small* **2022**, *18*, No. 2201667.

(3) Mandal, N.; Pramanik, A.; Dey, A.; Kumbhakar, P.; Kochat, V.; Gautam, A. R. S.; Glavin, N.; Roy, A. K.; Ajayan, P. M.; Tiwary, C. S. Synthesis of atomically thin yellow pearl: An impetus for nonlinear optical effect assisted light scattering application. *Opt. Mater.* **2023**, *135*, No. 113325.

(4) Bindi, L.; Feng, T.; Pasek, M. A. Routes to Reduction of Phosphate by High-energy Events. *Commun. Earth Environ.* **2023**, *4*, No. 70.

(5) Reibold, M.; Paufler, P.; Levin, A.; Kochmann, W.; Pätzke, N.; Meyer, D. C. Carbon Nanotubes in an Ancient Damascus Sabre. *Nature* **2006**, *444*, No. 286.

(6) Reiche, I.; Müller, K.; Albéric, M.; Scharf, O.; Wähning, A.; Bjeoumikhov, A.; Radtke, M.; Simon, R. Discovering Vanished Paints and Naturally Formed Gold Nanoparticles on 2800 Years Old Phoenician Ivories Using SR-FF-MicroXRF with the Color X-ray Camera. *Anal. Chem.* **2013**, *85*, 5857−5866.

(7) Cavallaro, G.; Milioto, S.; Lazzara, G. Halloysite Nanotubes: Interfacial Properties and Applications in Cultural Heritage. *Langmuir* **2020**, *36*, 3677−3689.

(8) Yuce, S.; Demirel, O.; Tas, B. A.; Sungur, P.; Unal, H. Halloysite Nanotube/Polydopamine Nanohybrids as Clay-Based Photothermal Agents for Antibacterial Applications. *ACS Appl. Nano Mater.* **2021**, *4*, 13432−13439.

(9) Pasbakhsh, P.; Churchman, G. J.; Keeling, J. L. Characterisation of Properties of Various Halloysites Relevant to Their Use as Nanotubes and Microfibre Fillers. *Appl. Clay Sci.* **2013**, *74*, 47−57.

(10) Makaremi, M.; Pasbakhsh, P.; Cavallaro, G.; Lazzara, G.; Aw, Y. K.; Lee, S. M.; Milioto, S. Effect of Morphology and Size of Halloysite Nanotubes on Functional Pectin Bionanocomposites for Food Packaging Applications. *ACS Appl. Mater. Interfaces* **2017**, *9*, 17476−17488.

(11) Jana, S.; Kondakova, A. V.; Shevchenko, S. N.; Sheval, E. V.; Gonchar, K. A.; Timoshenko, V. Y.; Vasiliev, A. N. Halloysite Nanotubes with Immobilized Silver Nanoparticles for Anti-Bacterial Application. *Colloids Surf., B* **2017**, *151*, 249−254.

(12) Yang, X.; Zhang, Y.; Zheng, D.; Yue, J.; Liu, M. Nano-Biocomposite Films Fabricated from Cellulose Fibers and Halloysite Nanotubes. *Appl. Clay Sci.* **2020**, *190*, No. 105565.

(13) Ren, X.; Zhang, H.; Zhang, B.; Zhao, H.; Wu, Y.; Ba, X. Halloysite/phenol-formaldehyde Nanocomposites with Enhanced Mechanical Properties and Lowered Fire Zazard. *Appl. Clay Sci.* **2023**, *231*, No. 106743.

(14) Cavallaro, G.; Lazzara, G.; Massaro, M.; Milioto, S.; Noto, R.; Parisi, F.; Riela, S. Biocompatible poly(N-isopropylacrylamide)-halloysite Nanotubes for Thermoresponsive Curcumin Release. *J. Phys. Chem. C* **2015**, *119*, 8944−8951.
(15) Lin, X.; Feng, Y.; He, Y.; Ding, S.; Liu, M. Engineering Design of Asymmetric Halloysite/Chitosan/Collagen Sponge with Hydrophobic Coating for High-Performance Hemostasis Dressing. *Int. J. Biol. Macromol.* **2023**, *237*, No. 124148.
(16) Peixoto, D.; Pereira, I.; Pereira-Silva, M.; Veiga, F.; Hamblin, M. R.; Lvov, Y.; Liu, M.; Paiva-Santos, A. C. Emerging Role of Nanoclays in Cancer Research, Diagnosis, and Therapy. *Coord. Chem. Rev.* **2021**, *440*, No. 213956.
(17) Gorbachevskii, M. V.; Stavitskaya, A. V.; Novikov, A. A.; Fakhrullin, R. F.; Rozhina, E. V.; Naumenko, E. A.; Vinokurov, V. A. Fluorescent gold nanoclusters stabilized on halloysite nanotubes: in vitro study on cytotoxicity. *Appl. Clay Sci.* **2021**, *207*, No. 106106.
(18) Ajumobi, O.; Su, Y.; Farinmade, A.; Yu, L.; He, J.; Valla, J. A.; John, V. T. Integrating Halloysite Nanostraws in Porous Catalyst Supports to Enhance Molecular Transport. *ACS Appl. Nano Mater.* **2021**, *4*, 8455−8464.
(19) Sadjadi, S. Halloysite-Based Hybrids/Composites in Catalysis. *Appl. Clay Sci.* **2020**, *189*, No. 105537.
(20) Zu, L.; Chen, Y.; Xi, J.; Liu, W.; Feng, Y.; Zhang, Z.; Zhao, X.; Ma, Y.; Fang, Q.; Li, K.; Guo, T.; Liu, M.; Wu, H. In situ Tumor Cells Detection Using Nanotube-functionalized & Microfluidic-controlling Multiresonance Optical Fiber. *Sens. Actuators, B* **2023**, *393*, No. 134176.
(21) Yang, M.; Xiong, X.; He, R.; Luo, Y.; Tang, J.; Dong, J.; Lu, H.; Yu, J.; Guan, H.; Zhang, J.; Chen, Z.; Liu, M. Halloysite Nanotube-Modified Plasmonic Interface for Highly Sensitive Refractive Index Sensing. *ACS Appl. Mater. Interfaces* **2018**, *10*, 5933−5940.
(22) Kornilova, A. V.; Gorbachevskii, M. V.; Kuralbayeva, G. A.; Jana, S.; Novikov, A. A.; Eliseev, A. A.; Vasiliev, A. N.; Timoshenko, V. Y. Plasmonic Properties of Halloysite Nanotubes with Immobilized Silver Nanoparticles for Applications in Surface-Enhanced Raman Scattering. *Phys. Status Solidi (A)* **2019**, *216*, No. 1800886.
(23) Fidecka, K.; Rotiroti, N.; Giacoboni, J.; Cámara, F.; Réfrégiers, M.; Vago, R.; Licandro, E.; Jamme, F. Second-Harmonic Generation of Halloysite Nanotubes for Bioimaging. *ACS Appl. Nano Mater.* **2021**, *4*, 4351−4355.
(24) Lvov, Y. M.; Shchukin, D. G.; Möhwald, H.; Price, R. R. Halloysite Clay Nanotubes for Controlled Release of Protective Agents. *ACS Nano* **2008**, *2*, 814−820.
(25) Padiyakkuth, N.; Antoine, R.; Kalarikkal, N. Random Lasing in Rhodamine 6G dye - Kaolinite Nanoclay Colloids Under Single Shot Nanosecond Pumping. *Opt. Mater.* **2022**, *129*, No. 112408.
(26) Wiersma, D. S. The Physics and Applications of Random Lasers. *Nat. Phys.* **2008**, *4*, 359−367.
(27) Tian, J.; Weng, G.; Wang, Y.; Hu, X.; Chen, S.; Chu, J. Random Lasing in ZnO Nanopowders Based on Multiphoton Absorption for Ultrafast Upconversion Application. *ACS Appl. Nano Mater.* **2019**, *2*, 1909.
(28) Xu, B.; Gao, Z.; Yang, S.; Sun, H.; Song, L.; Li, Y.; Zhang, W.; Sun, X.; Wang, Z.; Wang, X.; Meng, X. Multicolor Random Lasers Based on Perovskite Quantum Dots Embedded in Intrinsic Pb-MOFs. *J. Phys. Chem. C* **2021**, *125*, 25757−25764.
(29) Sznitko, L.; Mysliwiec, J.; Miniewicz, A. The role of polymers in random lasing. *J. Polym. Sci., Part B: Polym. Phys.* **2015**, *53*, 951−974.
(30) Roy, P. K.; Haider, G.; Lin, H. I.; Liao, Y. M.; Lu, C. H.; Chen, K. H.; Chen, L. C.; Shih, W. H.; Liang, C. T.; Chen, Y. F. Multicolor Ultralow-Threshold Random Laser Assisted by Vertical Graphene Network. *Adv. Opt. Mater.* **2018**, *6*, No. 1800382.
(31) Redding, B.; Choma, M. A.; Cao, H. Speckle-Free Laser Imaging Using Random Laser Illumination. *Nat. Photonics* **2012**, *6*, 355−359.
(32) de Souza, M. A. F.; Lencina, A.; Vaveliuk, P. Controlling Bichromatic Emission in Scattering Gain Media. *Opt. Lett.* **2006**, *31*, 1244−1246.
(33) Marinho, S. J.; Jesus, L. M.; Barbosa, L. B.; Ardila, D. R.; Alencar, M. A. R. C.; Rodrigues, J. J., Jr. Bi-chromatic Random Laser from Alumina Porous Ceramic Infiltrated with Rhodamine B. *Laser Phys. Lett.* **2015**, *12*, No. 055801.
(34) Gomes, A. S. L.; Carvalho, M. T.; Dominguez, C. T.; de Araujo, C. B.; Prasad, P. N. Direct Three-Photon Excitation of Up-Conversion Random Laser Emission in a Weakly Scattering Organic Colloidal System. *Opt. Express* **2014**, *22*, 14305−14310.
(35) Pincheira, P. I. R.; Silva, A. F.; Fewo, S. I.; Carreno, S. J. M.; Moura, A. L.; Raposo, E. P.; Gomes, A. S. L.; de Araujo, C. B. Observation of photonic paramagnetic to Spin-glass Transition in a Specially Designed TiO_2 Particle-based Dye-colloidal Random Laser. *Opt. Lett.* **2016**, *41*, 3459−3462.
(36) Ghofraniha, N.; Viola, I.; Dimaria, F.; Barbarella, G.; Gigli, G.; Leuzzi, L.; Conti, C. Experimental Evidence of Replica Symmetry Breaking in Random Lasers. *Nat. Commun.* **2015**, *6*, No. 6058.
(37) Sarkar, A.; Bhakta, B. N. S. Replica Symmetry Breaking in Coherent and Incoherent Random Lasing Modes. *Opt. Lett.* **2021**, *46*, 5169−5172.
(38) Hlil, A. R.; Lima, B. C.; Thomas, J.; Boisvert, J. S.; Iden, H.; Garcia-Puente, Y.; Maia, L. J. Q.; Ledemi, Y.; Messaddeq, Y.; Gomes, A. S. L.; Kashyap, R. Rare Earth Doped PDMS Elastomeric Random Lasers. *Opt. Mater.* **2019**, *97*, No. 109387.
(39) Xia, J.; Zhang, X.; Zhou, K.; Zhang, L.; Wang, E.; Du, W.; Ma, J.; Li, S.; Xie, K.; Yu, B.; Zhang, J.; Hu, Z. Tunable Replica Symmetry Breaking in Random Laser. *Nanophotonics* **2023**, *12*, 761−771.
(40) Lawandy, N. M.; Balachandran, R. M.; Gomes, A. S. L.; Sauvain, E. Laser Action in Strongly Scattering Media. *Nature* **1994**, *368*, 436−438.
(41) Sarkar, A.; Venkataraj, R.; Nampoori, V. P. N.; Kailasnath, M. Silver Nanoparticles Filled Hollow Polymer Fiber Laser with Enhanced Photostability. *Opt. Laser Technol.* **2019**, *112*, 255−260.
(42) Hari, M.; Joseph, S. A.; Mathew, S.; Nithyaja, B.; Nampoori, V.; Radhakrishnan, P. Thermal Diffusivity of Nanofluids Composed of Rod-Shaped Silver Nanoparticles. *Int. J. Therm. Sci.* **2013**, *64*, 188−194.
(43) Pincheira, P. I. R.; da Silva Neto, M. L.; Maldonado, M.; de Araujo´, C. B.; Jawaid, A. M.; Busch, R.; Ritter, A. J.; Vaia, R. A.; Gomes, A. S. L. Monolayer 2D $ZrTe_2$ transition metal dichalcogenide as nanoscatter for random laser action. *Nanoscale* **2020**, *12*, 15706−15710.
(44) Song, S.; Qiu, F.; Zhu, W.; Guo, Y.; Zhang, Y.; Ju, Y.; Feng, R.; Liu, Y.; Chen, Z.; Zhou, J.; Xiong, C.; Dong, L. Polyethylene glycol/halloysite@Ag Nanocomposite PCM for Thermal Energy Storage: Simultaneously High Latent Heat and Enhanced Thermal Conductivity. *Sol. Energy Mater. Sol. Cells* **2019**, *193*, 237−245.
(45) Cavallaro, G.; Chiappisi, L.; Pasbakhsh, P.; Gradzielski, M.; Lazzara, G. A Structural Comparison of Halloysite Nanotubes of Different Origin by Small-Angle Neutron Scattering (SANS) and Electric Birefringence. *Appl. Clay Sci.* **2018**, *160*, 71−80.
(46) Bavali, A.; Rahmatpanahi, A.; Niknam, Z. Anisotropic Behavior of Random Lasing in a Highly Concentrated Dye Solution. *Opt. Express* **2022**, *30*, 15685−15696.
(47) Lisuzzo, L.; Cavallaro, G.; Milioto, S.; Lazzara, G. Halloysite Nanotubes as Nanoreactors for Heterogeneous Micellar Catalysis. *J. Colloid Interface Sci.* **2022**, *608*, 424−434.
(48) Stobiecka, M.; Hepel, M. Multimodal Coupling of Optical Transitions and Plasmonic Oscillations in Rhodamine B Modified Gold Nanoparticles. *Phys. Chem. Chem. Phys.* **2011**, *13*, 1131−1139.
(49) Gummaluri, V. S.; Krishnan, S. R.; Vijayan, C. Stokes Mode Raman Random Lasing in a Fully Biocompatible Medium. *Opt. Lett.* **2018**, *43*, 5865−5868.
(50) Luan, F.; Gu, B.; Gomes, A. S. L.; Yong, K-T.; Wen, S.; Prasad, P. N. Lasing in Nanocomposite Random Media. *Nano Today* **2015**, *10*, 168−192.
(51) Vieira, R. J. R.; Gomes, L.; Martinelli, J. R.; Wetter, N. U. Upconversion Luminescence and Decay Kinetics in a Diode-pumped Nanocrystalline Nd^{3+}:YVO_4 Random Laser. *Opt. Express* **2012**, *20*, 12487−12497.

https://doi.org/10.1021/acsanm.3c02840
ACS Appl. Nano Mater. 2023, 6, 15896−15905

(52) Selvam, C.; Lal, D. M.; Harish, S. Thermal Conductivity Enhancement of Ethylene Glycol and Water with Graphene Nanoplatelets. *Thermochim. Acta* **2016**, *642*, 32−38.
(53) Khamliche, T.; Khamlich, S.; Doyle, T. B.; Makinde, D.; Maaza, M. Thermal Conductivity Enhancement of Nano-silver Particles Dispersed Ethylene Glycol Based Nanofluids. *Mater. Res. Express* **2018**, *5*, No. 035020.
(54) Biswas, S.; Kumbhakar, P. Continuous Wave Random Lasing in Naturally Occurring Biocompatible Pigments and Reduction of Lasing Threshold using Triangular Silver Nanostructures as Scattering Media. *Nanoscale* **2017**, *9*, 18812−18818.
(55) Okamoto, T.; Masaki, M. Random Laser Action in Dye-Doped Polymer Media with Inhomogeneously Distributed Particles and Gain. *Appl. Sci.* **2019**, *9*, No. 3499.
(56) Okamoto, T.; Imamura, K.; Kajisa, K. Inverse Design of Two-dimensional Disordered Structures for Spectral Optimization of Random Lasers. *Opt. Commun.* **2022**, *508*, No. 127775.
(57) Ni, D.; Späth, M.; Klämpfl, F.; Hohmann, M. Properties and Applications of Random Lasers as Emerging Light Sources and Optical Sensors: A Review. *Sensors* **2023**, *23*, No. 247.
(58) Mézard, M.; Parisi, G.; Virasoro, M. A. *Spin Glass Theory and Beyond: An Introduction to the Replica Method and Its Applications*; World Scientific Publishing Company, 1987; Vol. *9*.
(59) Choubey, P. S.; Varshney, S. K.; N, S. B. B. Glassy Behavior of Modes in Lasing Systems with Varying Openness: Random and Whispering Gallery Mode Lasers. *J. Opt. Soc. Am. B* **2022**, *39*, 3059−3065.

https://doi.org/10.1021/acsanm.3c02840
ACS Appl. Nano Mater. 2023, 6, 15896−15905